Heat Transfer and Performance Analysis of $NaMgH_2F$-based Thermochemical Energy Storage System

Sumeet Kumar Dubey[1], K. Ravi Kumar[1,*], Vinay Tiwari[2], and Umish Srivastva[2]

[1]Department of Energy Science and Engineering, Indian Institute of Technology (IIT) Delhi, New Delhi, India
[2]Department of Alternate Energy, Indian Oil Corporation R&D Centre, Faridabad, Haryana, India
Email: dubeysumeet92@gmail.com (S.K.D.); krk@dese.iitd.ac.in (K.R.K.); tiwarivd@indianoil.in (V.T.); srivastavau@indianoil.in (U.S.)
*Corresponding author
Manuscript received April 10, 2024; revised May 16, 2024; accepted June 8, 2024; published August 9, 2024

***Abstract*—Thermochemical energy storage systems are more suitable for high-temperature energy storage because of thermal stability and high energy storage density. Magnesium (Mg) based metal alloys and hydrides are found more suitable for high temperature energy storage applications among metal hydride-based thermochemical systems. The unit weight of $NaMgH_2F$ is used to analyze the energy sorption and heat transfer phenomenon. Initial metal hydride bed temperature variation and two heat transfer fluid flow arrangements are compared to study the heat transfer phenomenon and performance characteristics. The two initial metal hydride bed temperatures used in the analysis are 773 K and 823 K. Heat transfer flow configuration 1 has axial tubes in the cross-section, while Configuration 2 has a circumferential fluid jacket along with the axial tubes. Both configurations have the same heat transfer area for the comparative study of heat transfer. The energy absorption was not affected significantly, but the energy desorption increased with an increase in metal hydride bed temperature and with the outer circumferential cooling jacket configuration. The energy storage efficiency of 93.2% and 94.4% is obtained for initial metal hydride bed temperatures of 773 K and 823 K with flow Configuration 1, while the energy storage efficiency of 95.2% and 96.4% is obtained for 773 K and 823 K with flow Configuration 2.**

***Keywords*—thermochemical energy storage, metal hydrides, complex metal hydride, thermal battery, storage efficiency**

I. Introduction

Solar energy is one of the renewable sources that has the potential to address challenges such as increase in energy demand, greenhouse gas emissions, climate change, and depleting fossil fuel reserves. The diurnal and intermittent nature of solar energy is the biggest challenge in the continuous utilization of solar energy. Thermal Energy Storage (TES) systems help to overcome the challenge of continuous energy utilization. The different types of thermal energy storage systems with their characteristic properties are summarized in Fig. 1.

Thermochemical Energy Storage (TCES) systems store thermal energy in the form of endothermic chemical reactions and release the stored energy by reversing the chemical reaction. TCES systems are capable of storing large quantities of thermal energy at higher temperatures [1]. TES using Metal Hydrides (MH) are more famous because of their good chemical reversibility and high energy storage density. MH are classified as ionic, intermetallic, and complex metal hydrides. Ionic and some complex metal hydrides have high thermal stability, so they are suitable for high-temperature TES applications.

Magnesium-based hydrides are more popular among complex metal hydrides because of lower material cost, high energy storage density, high thermal stability, and good cyclic reversibility. One such complex MH is $NaMgH_2F$, which has a high enthalpy of reaction (96.8 kJ/mol) and is suitable for a temperature range of 500–600 °C.

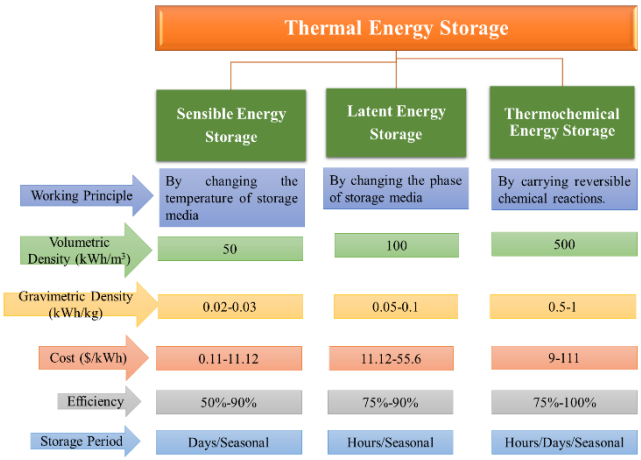

Fig. 1. Summary of thermal energy storage [2].

II. Literature Review

Several MH have been studied for TES applications, but Magnesium (Mg) based metal hydrides are found more suitable because of the lesser cost, easy availability, controlled reaction kinetics, and high storage density [3]. Some of the experimental scale models using Mg-based metal hydrides are also studied. A small-scale model of Mg hydride using 19 gm of MgH_2 was studied and energy storage at 420 °C was reported [4]. The model performed effectively without significant loss in energy storage capacity for 20 cycles. The authors reported significant heat losses, but it was expected to reduce with an increase in the model size. Mg-based alloys such as Mg-Ni, Mg-Fe, and Mg-Co were synthesized by using dopants such as Ni, Fe, and Co in Mg [5]. These dopants have improved the thermal and cyclic stability of the system. Ni alloyed Mg was studied, and its performance characteristics were compared with pure MgH_2 [6]. The thermal and cyclic stability of the Mg-Ni alloy was found better than pure Mg based hydride. Many studies have considered dual MH-based TES systems for performance and feasibility analysis. Dual metal hydride systems store thermal energy in High-Temperature Metal Hydride (HTMH), while hydrogen released from HTMH is stored in Low-Temperature Metal Hydride (LTMH). Mg-Fe alloy and sodium alanate were used as HTMH and LTMH, respectively [7]. The authors verified the feasibility of the

system for the temperature range of 450 to 500 ℃ and 132 kWh/m^3 energy storage density was reported. In another study, $NaMgH_2F$ and $TiCr_{1.6}Mn_{0.2}$ were used for coupled MH-based TES system [8]. The system storage density of 226 kWh/m^3 was reported in the study. Fin incorporated on $NaMgH_2F$ and $TiCr_{1.6}Mn_{0.2}$ based dual MH bed system was studied [9]. The study reported 90 kWh/m^3 of energy storage density with a storage efficiency of 96%. Another study used Mg-Ni alloy as HTMH and La-Ni alloy as LTMH for dual MH-based TES systems [10]. The energy storage density of 156 kWh/m^3 was reported, with energy storage efficiency of 89.4%. Mg-based hydrides are extensively studied and reported as suitable for the temperature 250–550 ℃ [5, 6, 11–13].

The present study used a unit weight of $NaMgH_2F$ for energy sorption and heat transfer analysis. The analysis studies the variation of initial MH bed temperature and two flow configurations. The two initial bed temperatures of MH selected for the analysis are 773 K and 823 K. The two flow configurations, namely flow Configurations 1 and 2, have the same heat transfer area but different flow arrangements. Configuration 1 has axial flow tubes in the cross-section domain, while Configuration 2 has a circumferential heat jacket along with axial tubes in the cross-section domain. The effect of change in the flow configuration and initial MH bed temperature on performance characteristics and heat transfer phenomenon is studied.

III. Numerical Modelling

The numerical model is developed using heat transfer in porous media and free and porous media flow modules of COMSOL Multiphysics. Multiphysics non-isothermal flow module is used to couple the heat transfer and fluid flow modules. The governing equation used in the model development are discussed and details of the governing equations can be referred from the author's published work [14].

Mass balance for MH bed

$$\varepsilon\frac{\partial\rho_h}{\partial t}+\nabla.(\rho_h u_h)=-S_m \quad (1)$$

$$(1-\varepsilon)\frac{\partial\rho_s}{\partial t}=S_m \quad (2)$$

$$S_m=C_a\exp\left(\frac{-E_a}{RT}\right)\left(\frac{p-p_{eq}}{p_{eq}}\right)(\rho_s-\rho_{s,emp})$$

for energy absorption ($p < p_{eq}$) (3)

$$S_m=C_d\exp\left(\frac{-E_d}{RT}\right)\ln\left(\frac{p}{p_{eq}}\right)(\rho_{s,sat}-\rho_s)$$

for energy desorption ($p > p_{eq}$) (4)

$$\ln\left(\frac{p}{p_{eq}}\right)=A-\frac{B}{T} \quad (5)$$

Mass balance for hydrogen in supply tube:

$$\frac{\partial\rho_h}{\partial t}+\nabla.(\rho_h u_h)=0 \quad (6)$$

Mass balance for heat transfer fluid:

$$\frac{\partial\rho_{HTF}}{\partial t}+\nabla.(\rho_{HTF}u_{HTF})=0 \quad (7)$$

Momentum balance for MH bed:

$$\frac{\rho_h}{\varepsilon}\left(\frac{\partial u_h}{\partial t}+u_h.\frac{\nabla u_h}{\varepsilon}\right)=-\nabla p+\nabla.\left[\frac{\mu_h}{\varepsilon}(\nabla u_h+(\nabla u_h)^T)-\frac{2}{3}\frac{\mu_h}{\varepsilon}(\nabla.u_h)\right]-\frac{\mu_h}{K}u_h+\frac{S_m}{\varepsilon^2}u_h \quad (8)$$

Momentum balance for hydrogen in supply tube:

$$\rho_h\left(\frac{\partial u_h}{\partial t}+u_h.\nabla u_h\right)=-\nabla p+\nabla.\left[\mu_h(\nabla u_h+(\nabla u_h)^T)-\frac{2}{3}\mu_h(\nabla.u_h)\right] \quad (9)$$

Momentum balance for heat transfer fluid:

$$\rho_{HTF}\left(\frac{\partial u_{HTF}}{\partial t}+u_{HTF}.\nabla u_{HTF}\right)=-\nabla p+\nabla.\left[\mu_{HTF}(\nabla u_{HTF}+(\nabla u_{HTF})^T)-\frac{2}{3}\mu_{HTF}(\nabla.u_{HTF})\right] \quad (10)$$

Energy balance for MH bed:

$$(\rho c_p)_{eff}\frac{\partial T}{\partial t}+\rho c_{ph}(u_h.\nabla T)=\nabla.(\sigma_{eff}\nabla T)+S_T \quad (11)$$

$$(\rho c_p)_{eff}=\varepsilon(\rho c_p)_h+(1-\varepsilon)(\rho c_p)_s \quad (12)$$

$$\sigma_{eff}=\varepsilon\sigma_h+(1-\varepsilon)\sigma_s \quad (13)$$

$$S_T=S_m(\Delta h) \quad (14)$$

Energy balance for hydrogen in supply tube:

$$(\rho_h c_{ph})\left(\frac{\partial T}{\partial t}+u_h.\nabla T\right)=\nabla.(\sigma_h\nabla T) \quad (16)$$

Energy balance for heat transfer fluid:

$$(\rho_{HTF}c_{pHTF})\left(\frac{\partial T}{\partial t}+u_{HTF}.\nabla T\right)=\nabla.(\sigma_{HTF}\nabla T) \quad (17)$$

The computational domain geometry of two fluid flow arrangements is shown in Fig. 2. Fig. 2(a) represents the fluid flow Configuration 1, while Fig. 2(b) represents the fluid flow Configuration 2.

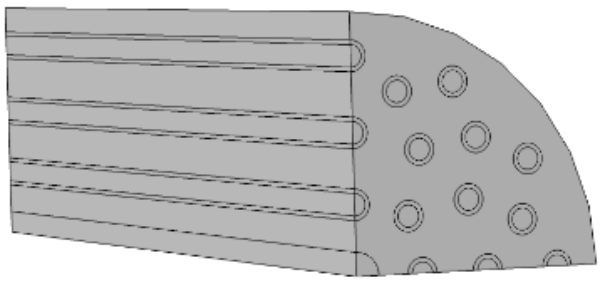

(a)

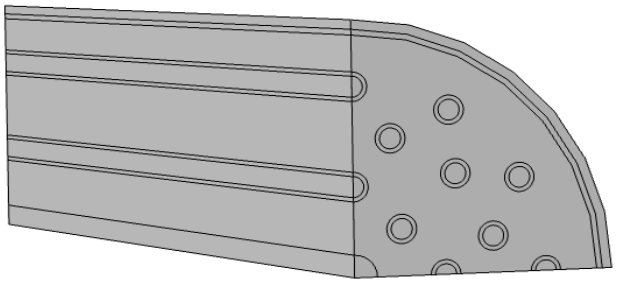

(b)

Fig. 2. Computational domain geometry used for the investigation (a) Configuration 1 and (b) Configuration 2.

The outer diameter of the MH bed for Configurations 1 and 2 are 10.32 and 10.16 cm, respectively, while the length of the MH bed for Configurations 1 and 2 are 20.64 and 20.32 cm, respectively. The Number of HTF tubes in Configuration 1 is 44, while Configuration 2 has 32 HTF tubes along with the HTF jacket at the outer periphery of the MH bed. The total surface area included in the heat transfer is maintained constant for both configurations. The HTF tubes have inner and outer diameters of 0.44 and 0.64 cm, respectively. The hydrogen tube at the center has a diameter of 0.95 cm.

The properties used in the numerical investigations are listed in Table 1.

Table 1. Properties used in numerical analysis

Properties	Value
Absorption/Desorption reaction rate constant	1000000/120000 (1/s)
Absorption/Desorption activation energy	151500/102500 (J/mol)
Absorption and Desorption reaction enthalpy	96800 (J/mol)
Absorption and Desorption reaction entropy	138 (J/mol K)
Universal gas constant	8.314 (J/mol K)
Empty MH reactor density	1390 (kg/m3)
Saturated MH reactor density	1424.7 (kg/m3)
MH bed thermal conductivity	0.5 (W/m K)

The initial MH temperatures considered for the analysis are 773 K and 823 K. The initial temperature of HTF is taken the same as the MH temperature. The initial pressure of the MH bed is considered the same as the equilibrium pressure corresponding to the two initial temperatures. The temperature of hydrogen supplied/rejected to/from MH is 298 K. The initial pressure of hydrogen and HTF are considered as 1 bar. The exposed surface of reactors is considered as insulated so that there is no heat loss from the reactor to the environment. The hydrogen gas flowing in the pores is considered ideal. The HTF is assumed as Newtonian fluid, and the properties of the materials are not temperature dependent.

IV. Results and Discussions

The developed model is validated for the physics used in the model development with the numerical results of Chung and Ho [15] and the experimental results of Jemni *et al.* [16]. Fig. 3(a) represents the model validation with Chung and Ho for energy absorption while Fig. 3(b) represents the model validation with Chung, Ho and Jemni *et al.* [15, 16] for energy desorption. The maximum deviation of temperature measured at a point is less than 2%.

The grid-independent study has been performed and 145,860 number of elements with an average element quality of 0.8531 are considered for the analysis. A physics-controlled adaptive time step size is used for the analysis, which automatically controls the time step size based on the physics used.

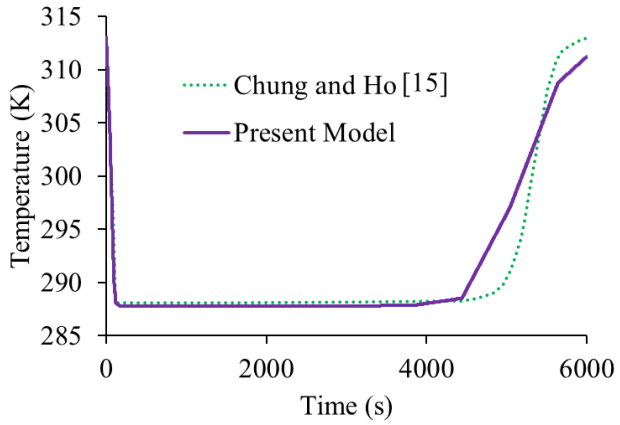

(a)

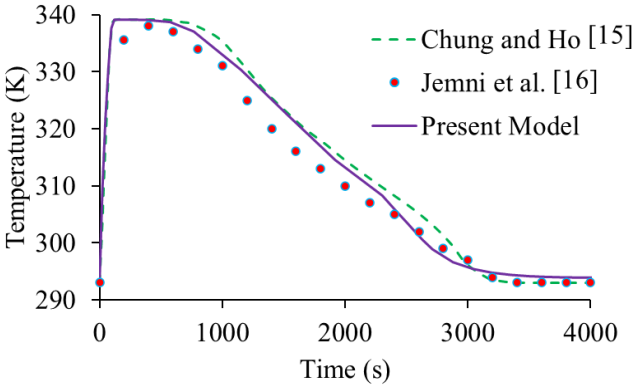

(b)

Fig. 3. Model validation for (a) energy absorption and (b) energy desorption.

The results of the analysis are divided into two sections, namely energy absorption and energy desorption. The energy absorption reaction is found to be very slow and therefore, the result analysis for energy absorption is not very informative as compared to energy desorption. Therefore, the result and discussion section have the majority of results included from energy desorption analysis; however, results of energy absorptions are also discussed in this study.

A. *Energy Absorption*

The average MH bed temperature and density variation for energy absorption are studied. With the increase in MH bed temperature, the reaction kinetics has increased and the heat absorption in MH bed has increased. Thus, saturation of the MH bed at lower temperatures is achieved slower than the MH bed at higher temperatures. The reaction kinetics of the absorption process is too slow as compared to the energy desorption. Due to very slow energy absorption reaction kinetics, the two flow configurations have no significant variations. However, the MH bed with flow Configuration 2 has shown relatively uniform temperature in the MH bed cross-section, as indicated in the temperature contours in Figs. 4 and 5.

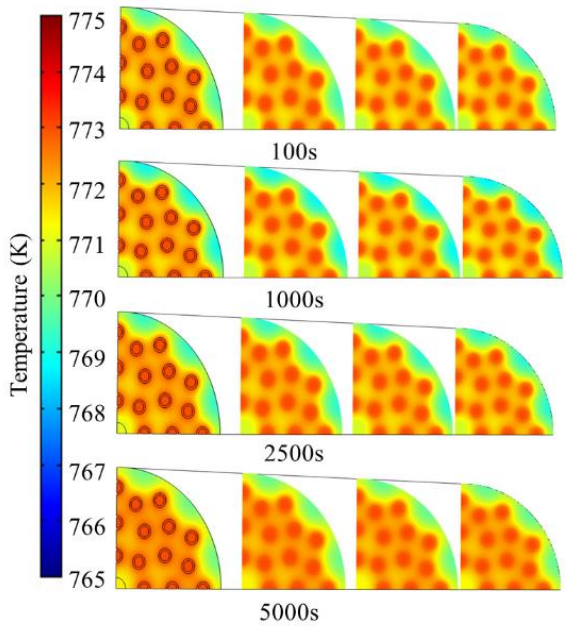

(a)

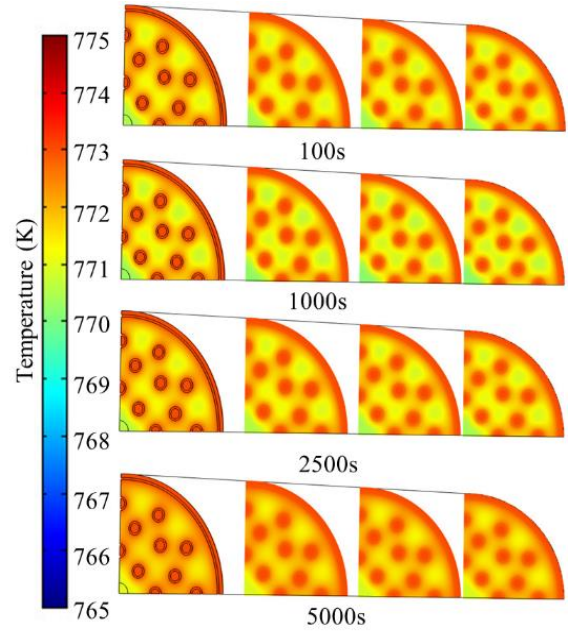

(b)

Fig. 4. Temperature contours for 773 K initial MH bed temperature for (a) Configuration 1 and (b) Configuration 2 during energy absorption.

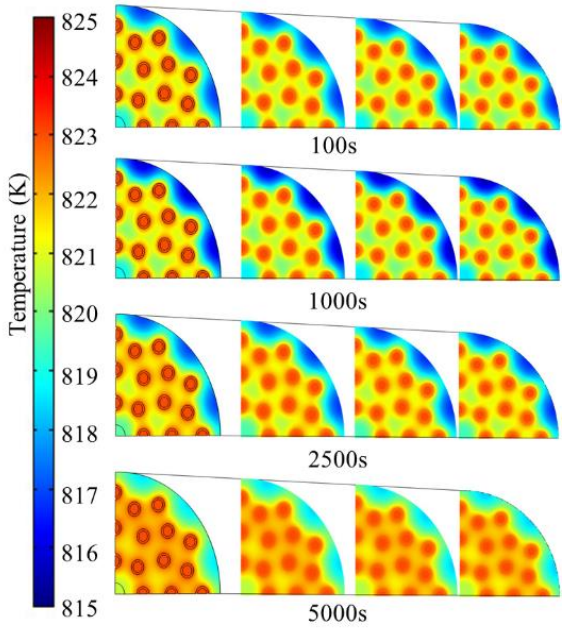

(a)

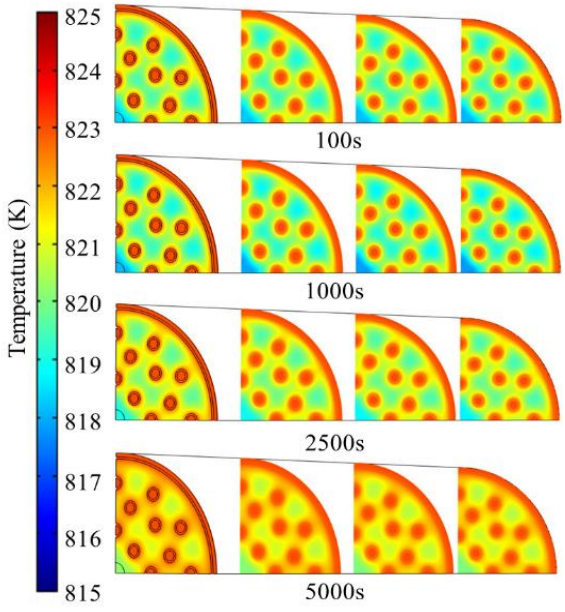

(b)

Fig. 5. Temperature contours for 8233 K initial MH bed temperature for (a) Configuration 1 and (b) Configuration 2 during energy absorption.

Fig. 4(a) and (b) represent the temperature contour of the MH bed at 773 K for Configurations 1 and 2, respectively. Fig. 5(a) and (b) represent the temperature contour of the MH bed at 823 K for Configurations 1 and 2, respectively. At any instant, the temperature in the cross-section domain is more uniform for flow Configuration 2. The saturation of the MH bed at higher temperatures is faster, while flow Configuration 2 has achieved the saturation faster.

The energy absorbed in the MH bed at 773 K for fluid flow Configurations 1 and 2 is 241.01 kJ and 241.73 kJ, respectively. The energy absorbed in the MH bed at 823 K for fluid flow Configurations 1 and 2 is 254.18 kJ and 254.98 kJ, respectively.

B. Energy Desorption

The variation of MH bed temperature, density, and energy desorbed from the MH bed is studied in this analysis. The MH average bed temperature for two different cases of initial MH bed temperature and two HTF flow configurations are shown in Fig. 6. The curve in red and purple color represents the results for initial MH bed temperatures of 773 K and 823 K respectively. The solid and dotted lines represent the results of HTF flow Configurations 1 and 2, respectively. Fluid flow Configuration 2 has achieved a steady state faster than flow Configuration 2. The outer fluid jacket in configuration 2 has provided an additional heat extraction effect and thus, the MH has achieved steady state relatively faster. The effect of the circumferential jacket can be seen in the temperature variation near the steady state.

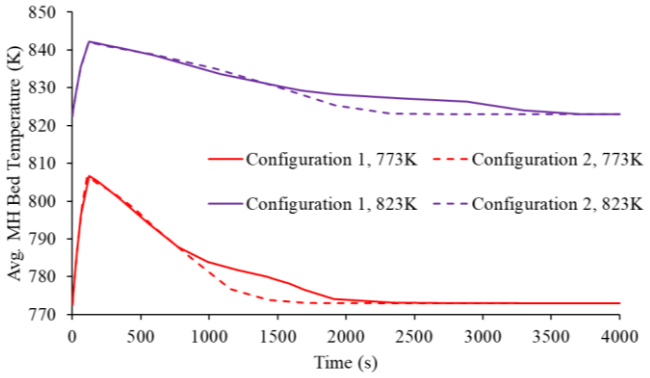

Fig. 6. Average MH bed temperature variation for different initial MH bed temperatures and HTF flow configuration during energy desorption.

The MH bed density variation for two different cases of initial MH bed temperature and two HTF flow configurations are shown in Fig. 7. The addition of hydrogen during energy desorption results in an increase in the MH bed density. The bed with flow Configuration 2 for both cases of initial MH bed temperature has achieved saturation faster. The reaction rate is faster for the bed at higher temperatures and the heat generation from the bed is high. The heat extraction from the bed with flow Configuration 2 is higher and therefore, it achieves the steady state faster in Fig. 7.

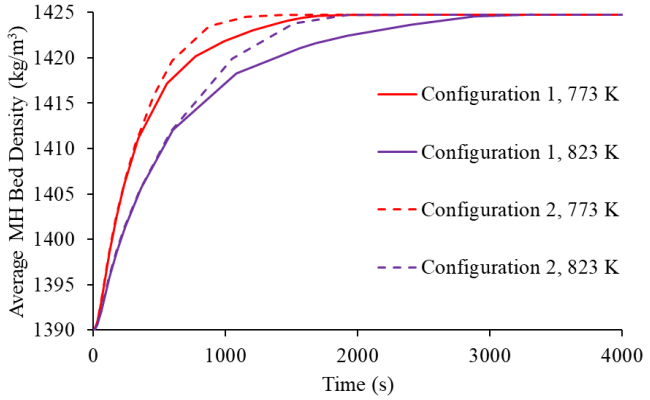

Fig. 7. Average MH bed density variation for different initial MH bed temperatures and HTF flow configuration during energy desorption.

The energy desorbed from the MH bed at 773 K for fluid flow Configurations 1 and 2 are 224.54 kJ and 230.20 kJ, respectively. The energy desorbed from the MH bed at 823 K for fluid flow Configurations 1 and 2 are 239.99 kJ and 245.92 kJ, respectively. The total energy released from the MH bed with flow Configuration 2 is higher than flow Configuration 1.

The density contours of the two flow configurations are compared in Fig. 8. Fig. 8(a) represents the density contours at 773 K and 823 K for flow Configuration 1. Fig. 8(b) represents the density contours at 773 K and 823 K for flow Configuration 2. The MH bed at a particular temperature has achieved saturation faster with flow Configuration 2. The comparison of density at the two different temperatures with the same flow configuration shows that the bed at lower temperatures gets saturated faster.

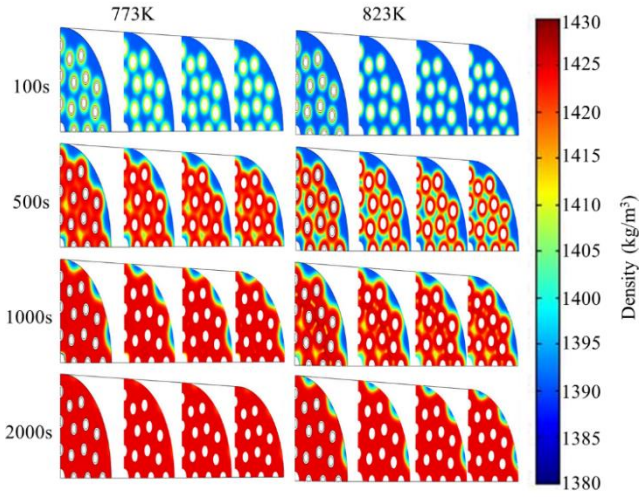

(a)

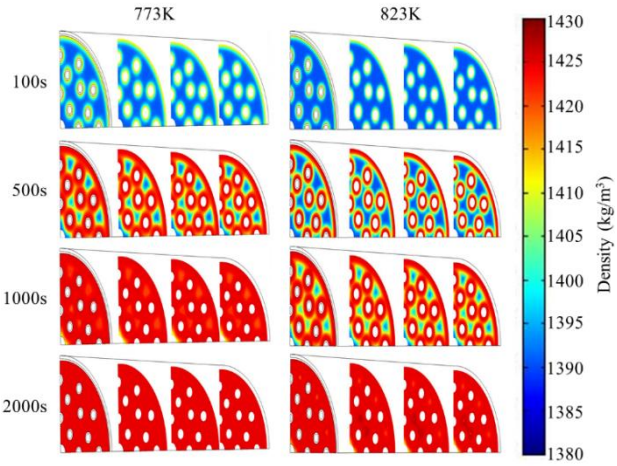

(b)

Fig. 8. Density contours for different initial MH bed temperatures for flow (a) Configuration 1 (b) Configuration 2.

The energy storage efficiency is defined as the ratio of energy desorbed to the energy absorbed for a particular case. The energy storage efficiency has shown a marginal increase in magnitude with an increase in the MH bed temperature, while the increase in efficiency is significant with a change in the flow configuration as shown in Fig. 9. The energy storage efficiency for MH bed temperature 773 K and 823 K for flow Configuration 1 is 93.2% and 94.4%, respectively. For flow Configuration 2, the energy storage efficiency for MH bed temperatures 773 K and 823 K are 95.2% and 96.4%.

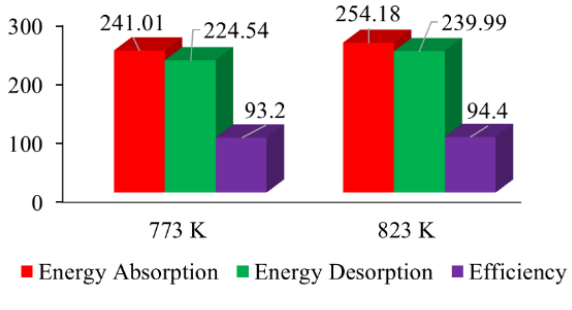

(a)

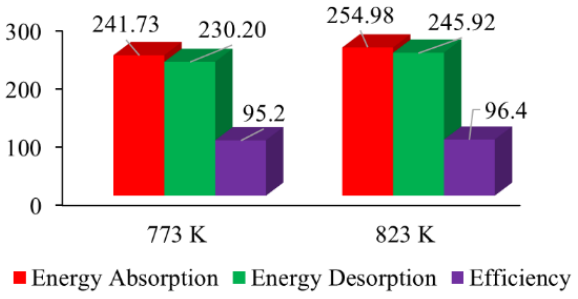

(b)

Fig. 9. Energy absorption, desorption, and storage efficiency at different initial MH bed temperatures for (a) Configuration 1 and (b) Configuration 2.

V. Conclusion

The performance characteristics and heat transfer analysis of energy storage and discharge have been performed in $NaMgH_2F$. The conclusions of the study are as follows.

- The reaction rate of energy absorption is too slow than the energy desorption process.
- The reaction rate increased with the temperature of the metal hydride bed and during energy desorption, flow configuration 2 is found effective for heat extraction.
- The energy desorption has increased slightly with the increase in metal hydride bed temperature, while there is no significant increase in the value of energy absorption.
- A significant increase in the energy desorption was observed with flow Configuration 2 than the flow Configuration 1.
- Energy storage efficiency has increased from 93.2% to 94.4% when metal hydride bed temperature is increased from 773 K to 823 K.
- Energy storage efficiency is found to be 95.2% to 96.4% with flow Configurations 1 and 2, respectively.

Conflict of Interest

The authors declare no conflict of interest.

Author Contributions

Sumeet Kumar Dubey: Conceptualization, Methodology, Investigation, Visualization, Writing—original draft. K. Ravi Kumar: Conceptualization, Investigation, Supervision, Writing—review & editing. Vinay Tiwari: Supervision, Draft review. Umish Srivastva: Supervision, Draft review. All authors had approved the final version.

Acknowledgment

The authors are thankful to the Science and Engineering Research Board (SERB), Department of Science and Technology (DST), Government of India, and Confederation of Indian Industry (CII) for awarding "Prime Minister Fellowship for Doctoral Research" to Mr. Sumeet Kumar Dubey in collaboration with Indian Oil Corporation Limited, Research and Development Centre.

References

[1] S. Jain, S. K. Dubey, K. R. Kumar, and D. Rakshit, "Thermal energy storage for solar energy," *Fundamentals and Innovations in Solar Energy*, pp. 167–215, 2021. doi: 10.1007/978-981-33-6456-1_9

[2] S. K. Dubey, K. R. Kumar, V. Tiwari, and U. Srivastva, "Impacts, barriers, and future prospective of metal hydride-based thermochemical energy storage system for high-temperature applications : A comprehensive review," *Energy Technol.*, vol. 12, 2300768, pp. 1–28, 2024, doi: 10.1002/ente.202300768.

[3] B. Bogdanović, A. Ritter, B. Spliethoff, and K. Straßburger, "A process steam generator based on the high temperature magnesium hydride/magnesium heat storage system," *International Journal of Hydrogen Energy*, vol. 20, no. 10, pp. 811–822, 1995. doi: 10.1016/0360-3199(95)00012-3

[4] M. Paskevicius, D. A. Sheppard, K. Williamson, and C. E. Buckley, "Metal hydride thermal heat storage prototype for concentrating solar thermal power," *Energy*, vol. 88, pp. 469–477, 2015. doi: 10.1016/j.energy.2015.05.068

[5] A. Reiser, B. Bogdanović, and K. Schlichte, "Application of Mg-based metal-hydrides as heat energy storage systems," *International Journal of Hydrogen Energy*, vol. 25, no. 5, pp. 425–430, 2000. doi: 10.1016/S0360-3199(99)00057-9

[6] B. Bogdanovic, H. Hofmann, A. Neuy, A. Reiser, K. Schlichte, B. Spliethoff, and S. Wessel, "Ni-doped versus undoped Mg-MgH2 materials for high temperature heat or hydrogen storage," *Journal of Alloys and Compounds*, vol. 292, no. 1–2, pp. 57–71, 1999. doi: 10.1016/S0925-8388(99)00109-7

[7] A. D'Entremont., C. Corgnale, M. Sulic, B. Hardy, R. Zidan, and T. Motyka, "Modeling of a thermal energy storage system based on coupled metal hydrides (magnesium iron-sodium alanate) for concentrating solar power plants," *International Journal of Hydrogen Energy*, vol. 42, no. 35, pp. 22518–22529, 2017. doi: 10.1016/j.ijhydene.2017.04.231

[8] A. D'Entremont, C. Corgnale, B. Hardy, and R. Zidan, "Simulation of high temperature thermal energy storage system based on coupled metal hydrides for solar driven steam power plants," *International Journal of Hydrogen Energy*, vol. 43, no. 2, pp. 817–830, 2018. doi: 10.1016/j.ijhydene.2017.11.100

[9] S. Mellouli, F. Askri, A. Edacherian, T. Alqahtani, S. Algarni, J. Abdelmajid, and P. Phelan, "Performance analysis of a thermal energy storage based on paired metal hydrides for concentrating solar power plants," *Applied Thermal Engineering*, vol. 144, pp. 1017–1029, 2018. doi: 1037//0033-2909.I26.1.78

[10] K. Malleswararao, A. N, S. S. Murthy, and P. Dutta, "Performance prediction of a coupled metal hydride based thermal energy storage system," *International Journal of Hydrogen Energy*, vol. 45, no. 32, pp. 16239–16253, 2020. doi: 10.1016/j.ijhydene.2020.03.251

[11] S. K. Dubey and K. R. Kumar, "Numerical investigation of energy desorption from magnesium nickel hydride based thermal energy storage system," *Journal of Energy Systems*, vol. 6, no. 2, pp. 165–175, 2022. doi: 10.30521/jes.952627

[12] S. K. Dubey and K. R. Kumar, "Numerical investigation of energy desorption from magnesium nickel hydride based thermal energy storage," in *Proc. 9th Eur. Conf. Ren. Energy Sys.*, 2021, pp. 457–462.

[13] S. K. Dubey and K. R. Kumar, "Numerical investigation of thermal energy storage using magnesium nickel hydride," in *Proc. 26th National and 4th International ISHMT-ASTFE Heat and Mass Transfer Conference*, 2021, pp. 577–583. doi: 10.1615/IHMTC-2021.870

[14] S. K. Dubey and K. R. Kumar, "Charging and discharging analysis of thermal energy using magnesium nickel hydride based thermochemical energy storage system," *Sustainable Energy Technologies and Assessments*, vol. 52, no. PA, 101994, 2022. doi: 10.1016/j.seta.2022.101994

[15] C. A. Chung and C. J. Ho, "Thermal-fluid behavior of the hydriding and dehydriding processes in a metal hydride hydrogen storage canister," *International Journal of Hydrogen Energy*, vol. 34, no. 10, pp. 4351–4364, 2009. doi: 10.1016/j.ijhydene.2009.03.028

[16] A. Jemni, S. Ben Nasrallah, and J. Lamloumi, "Experimental and theoretical study of a metal-hydrogen reactor," *International Journal of Hydrogen Energy*, vol. 24, no. 7, pp. 631–644, 1999. doi: 10.1016/S0360-3199(98)00117-7